

Enhancing thermoelectric figure-of-merit by low-dimensional electrical transport in phonon-glass crystals

Xue-Ya Mi,^{†,⊥} Xiaoxiang Yu,^{‡,⊥} Kai-Lun Yao,[†] Xiaoming Huang,[¶] Nuo Yang,^{*,‡,§}
and Jing-Tao Lü^{*,†,||}

School of Physics and Wuhan National High Magnetic Field Center, Huazhong University of Science and Technology, Wuhan 430074, P. R. China, Nano Interface Center for Energy (NICE), School of Energy and Power Engineering, Huazhong University of Science and Technology, Wuhan 430074, P. R. China, School of Energy and Power Engineering, Huazhong University of Science and Technology, Wuhan 430074, P. R. China, State Key Laboratory of Coal Combustion, Huazhong University of Science and Technology, Wuhan 430074, China, and Beida Information Research, Tianjin 300457, China

E-mail: nuo@hust.edu.cn; jtlu@hust.edu.cn

Abstract

Low-dimensional electronic and glassy phononic transport are two important ingredients of highly-efficient thermoelectric material, from which two branches of the thermoelectric research emerge. One focuses on controlling electronic transport in the low dimension, while

*To whom correspondence should be addressed

[†]School of Physics, HUST

[‡]NICE, School of Energy and Power Engineering, HUST

[¶]School of Energy and Power Engineering, Huazhong University of Science and Technology, Wuhan 430074, P. R. China

[§]State Key Laboratory of Coal Combustion, HUST

^{||}BIR

[⊥]These authors contributed equally to the work

the other on multiscale phonon engineering in the bulk. Recent work has benefited much from combining these two approaches, e.g., phonon engineering in low-dimensional materials. Here, we propose to employ the low-dimensional electronic structure in bulk phonon-glass crystal as an alternative way to increase the thermoelectric efficiency. Through first-principles electronic structure calculation and classical molecular dynamics simulation, we show that the π - π stacking Bis-Dithienothiophene molecular crystal is a natural candidate for such an approach. This is determined by the nature of its chemical bonding. Without any optimization of the material parameter, we obtain a maximum room-temperature figure of merit, ZT , of 1.48 at optimal doping, thus validating our idea.

Keywords: Thermoelectric Effect, Molecular Crystals, Electronic Structure Calculation, Molecular Dynamics Simulation

Introduction

The thermoelectric efficiency of a material is characterized by the dimensionless figure of merit $ZT = \sigma S^2 T / (\kappa_e + \kappa_{ph})$, with S the Seebeck coefficient, σ the electrical conductivity, κ_e the electron thermal conductivity, κ_{ph} the phonon thermal conductivity, and T the temperature. The optimization of ZT is a highly non-trivial task, e.g., the electrical conductivity and the electron thermal conductivity are, in many cases, related by the Wiedemann-Franz law.

Different strategies have been proposed to increase the ZT value.¹⁻⁴ In their seminal work, Hicks and Dresselhaus proposed to increase S utilizing the sharp change of electrical density of states (DOS) in low-dimensional structures,⁵⁻⁷ such as semiconductor quantum wells, quantum wires, quantum dots, and single molecular devices.^{3,4} Another approach is to search or design electron-crystal-phonon-glass materials by phonon engineering (phononics).^{8,9} The idea is to reduce the phonon thermal conductivity while keeping the electrical conductivity intact.¹ Recently, combining these two approaches, phonon engineering is used in low-dimensional structures, like silicon nanowires, to boost their ZT .¹⁰⁻¹⁴ A natural question then arises: Is it possible to do the opposite, utilizing low-dimensional electrical transport in bulk phonon-glass crystals? To show

this is indeed possible, we need to start from bulk materials with low thermal conductivity.

Thus far, the main focus of the thermoelectric research community is inorganic semiconductor materials,^{2,15} including Bi_2Te_3 ,¹⁶ PbTe ,¹⁷ SiGe ,¹⁸ SnSe ,¹⁹ perovskites,²⁰ and Si .^{21,22} Instead, we focus on organic semiconductors, especially molecular crystals, which have been intensively studied in the development of organic photovoltaic cells,²³ light-emitting diodes,²⁴ and field-effect transistors.^{25,26} Currently, their thermoelectric properties have received more attention.²⁷⁻³² Compared with inorganic materials, the advantages of organic thermoelectric materials are lightweight, flexible, cheap and easy to process over large areas.³³ Due to the weak bonding between different molecules, organic molecular crystals have natural low thermal conductivity. Recent experimental progress has resulted in several orders of magnitude increase of ZT , from $0.001 \sim 0.01$ ^{34,35} to 0.42 .^{36,37} Moreover, it is now possible to design and modulate the transport characteristics of organic structures.³¹ Among them, π - π stacking molecular crystals have proved their superior electronic transport properties along the development of organic field-effect transistors.²⁶ Interestingly, it has been shown that, their electronic transport properties can be controlled by tuning the stacking angle and distance.^{26,38}

Here, we attend to Bis-Dithienothiophene molecular crystal (BDTMC) which has the interesting electrochemical and optical properties.³⁹ As shown in Fig. 1(a), each dithienothiophene molecule possess three fused thiophene rings and they form crystal structure through π - π stacking. The way that small molecules stack together determines the structure and electronic property of the organic crystal. Herringbone stacking is one of the common stacking structures, whose electronic band structure is normally two-dimensional, as a result of π - π stacking extending in two dimensions. The BDTMC favors coplanar stacking⁴⁰ and has high mobility.^{28,40} Due to the strong π - π overlap only along one direction, it shows a quasi-one-dimensional (Q1D) band with a large band dispersion (Fig 1(a-b)). This Q1D band structure is different from common two-dimensional band in molecular crystals and appropriate for our study on thermoelectrics. Besides, its thermoelectric transport properties are under experimental investigation.⁴¹

Based on a general one-dimensional tight-binding model validated by Density Functional The-

ory (DFT), we employ the semi-classical Boltzmann transport theory to study its electronic transport properties. Meanwhile, the phonon thermal conductivity is calculated using the classical molecular dynamics (MD) simulation. We show that, Q1D electronic transport and phonon-glass-like thermal transport are realized at the same time in bulk BDT molecular crystal, which suggests a great thermoelectric potential for π - π stacking organic molecular crystals.

Results and Discussion

Electronic structure.

The lattice and electronic structure of BDTMC are calculated from Vienna Ab-initio Simulation Package (VASP).⁴² The Perdew-Burke-Ernzerhof (PBE) version of generalized gradient approximation (GGA) is used for the exchange-correlation potential.⁴³ The DFT-D2 method of Grimme is used to take into account the van der Waals (VDW) interactions between different molecules⁴⁴ (details in Supporting information (SI), I(A)). Figure 1(a) shows the relaxed structure. It forms a triclinic Bravais lattice, with two molecules within one primitive unit cell, shown in dashed lines. The conduction (CB), valence band (VB) structure and DOS are shown in Fig. 1(b) and (c). We observe a strong band dispersion along y direction, G-B-G, comparing to other directions. This indicates a large overlap of π orbitals between molecules along y direction, due to the small angle between y and the π - π stacking (π) direction. The band structure along y is well re-produced by a fitting using the dispersion of 1D tight-binding model (red dots). Model details are given in SI, II.

Due to a small electronic overlap between molecules in the same unit cell, the conduction and valence bands come in pairs, each mainly localized in one molecule. By comparing the charge distribution of the bands with the electronic states of the isolated molecule pair, we find that the VB and CB are simply formed by the highest occupied molecular orbitals (HOMOs) and lowest unoccupied molecular orbitals (LUMOs) of each molecule, respectively [Fig. 1 (d) and (e)]. The strong anisotropy in band dispersion suggests the formation of Q1D band structure along y direction. This is further supported by the van-Hove-like high DOS near the band edges [Fig. 1(c)]. For

1D system, the DOS is inversely proportional to the hopping element t . Thus, the DOS at valence band edge is around one-third of DOS at the conduction band edge. Hereafter, we focus on the electrical properties along y direction.

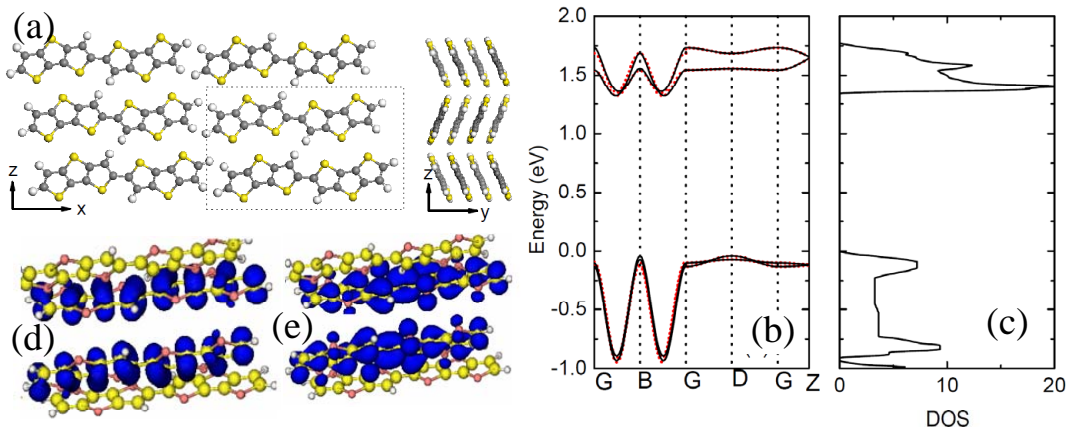


Figure 1: **The lattice and DFT band structure.** (a) The relaxed structure of the BDT crystal along different directions. The lattice vectors are: $a_1 = (16.82, 0.087, 0.015) \text{ \AA}$, $a_2 = (16.40, 3.85, 0.015) \text{ \AA}$, and $a_3 = (-2.08, -0.24, 10.68) \text{ \AA}$. The y -direction is approximately perpendicular to the molecular plane. (b)-(c) DFT band structure and density of states (DOS) of the BDT crystal. The energy zero is set to the top of the valence band. The reciprocal space coordinates of high-symmetry points are $G = (0, 0, 0)$, $B = (-0.5, 0.5, 0)$, $D = (0.5, 0.5, 0)$, and $Z = (0, 0, 0.5)$, in unit of the reciprocal lattice constants. The red dots represent the bands fitted using one-dimensional band dispersion $\varepsilon \sim -2t \cos(kL_0)$, with $t = -0.2, -0.2 \text{ eV}$ for the two valence bands, and $-0.05, -0.08 \text{ eV}$ for the two conduction bands (see text for details). (d) Charge density distribution of the two nearly degenerate HOMO orbitals in one isolated unit cell. They are localized in each molecule, and form the two valence bands in the lattice structure. (e) Corresponding LUMO orbitals forming the conduction bands.

The intrinsic transport mechanism in organic molecular crystals has been under active debate. Band and hopping models have been used to understand the experimental results.^{45,46} It is commonly accepted that band-like model should be used if the inter-molecular hopping element t is larger or comparable to the molecule reorganization energy λ .^{45,47} Following the method in Ref. 47, we obtained λ of $\sim 0.18 \text{ eV}$, comparable to t . Thus, we use the band model to study transport along y direction. This is also supported by the fact that hopping model predicts a mobility that is one-order-of-magnitude smaller than the experimental value in a similar molecular crystal.⁴⁸

Based on the band structure obtained from VASP,⁴² we use the BoltzTraP code⁴⁹ to calculate its contribution to the transport coefficients, e.g., $(\kappa_e + S^2\sigma T)/\tau$, $S^2\sigma/\tau$, with τ the constant relaxation time. Rigid band approximation is used to relate the Fermi level (E_f) position with the electron/hole doping concentration [Fig. 2(a)]. The weak dependence of E_f on doping within three decades is due to the van-Hove-like DOS at the band edges. Thus, similar to Q1D structure, we expect a high Seebeck coefficient shows up in the bulk molecular crystal. The DFT result is further compared with a 1D model calculation using the parameters obtained from fitting the band structure (Details in SI, I(A)). We find excellent agreement between the two approaches near the band edges [Fig. 2(b-c)]. This agreement validates the 1D model, which we will use in the following.

Electrical transport.

A common approach to obtain the thermoelectric transport coefficients based on the DFT plus BoltzTraP calculation is to use a constant τ . It is obtained either from fitting of the experiments, or from the theoretical estimation. To estimate the relaxation time, we need to consider different types of carrier scattering process. Defects, charge traps may scatter the carriers strongly, and even invalidate the band-like transport model used here. But these scatterings are extrinsic, and depend on the quality of the sample. The charged impurity scattering due to doping is another source of scattering. To take it account, we should consider the screening of the charged impurity, which is a problem that deserves separate study. Here, we only take into account the intrinsic scattering mechanism, namely the interaction of electrons with acoustic phonons, which is present independent on the quality of the sample. Due to the Q1D electronic structure, using the Bardeen-Shockley deformation potential theory,^{50,51} we go beyond the constant- τ approach by taking into account the k dependence of $\tau(k)$ (SI, II)

$$\frac{1}{\tau(k)} \approx \frac{k_B T D^2}{\hbar^2 C |v_k|}. \quad (1)$$

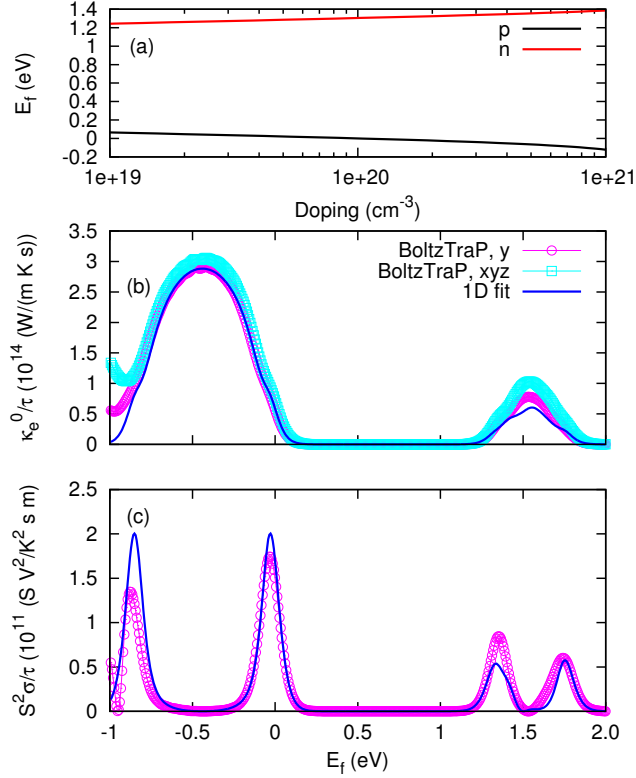


Figure 2: **DFT plus BoltzTraP calculation and model fitting.** (a) The Fermi level (E_f) as a function of electron (red) and hole (black) doping at $T = 300$ K. The weak dependence of the E_f on doping across three decades is characteristic of quasi-one-dimensional energy band. (b)-(c) The dependence of $\kappa_e^0/\tau = (\kappa_e + S^2\sigma T)/\tau$ and $S^2\sigma/\tau$ on E_f . The points are results from DFT plus BoltzTraP calculation, while the lines are from the 1D tight-binding model with the hopping element t fitted from the band structure in Fig. 1(b). In (b), xyz means summing up all three directions, while y means contribution from y direction only. As can be seen, the contributions from x and z are negligible.

Here, k_B is the Boltzmann constant, T is the temperature, $C = \partial^2 E / (L_0 \partial \Delta L^2)$ is the 1D elastic constant, with $\Delta L = \delta L / L_0$. $D = \Delta E / \Delta L$ is the deformation potential constant, with ΔE the energy shift of the valence or conduction band edge (SI, I(B)). This makes our approach different from the common BoltzTraP calculation, and much closer to the real situation. The relevant transport coefficients κ_e , σ are shown in Fig. 3(a) and (b). We see a better transport performance of the holes. It can be attributed to their larger hopping element t , leading to larger group velocity (SI, II). Moreover, a strong deviation of the Wiedemann-Franz law is observed in Fig. 3(c), typical at the band edges or low-dimensional structures. The smaller value of $\kappa_e / (T \sigma) < L$ indicates reduced electron thermal conductivity, and good thermoelectric performance.

Phonon transport.

To get ZT , we also need the phonon thermal conductivity κ_{ph} , which was calculated by equilibrium MD simulation using LAMMPS⁵² (Details in SI, III). The following results are obtained from a simulation cell of $4 \times 6 \times 4$ unit cells in x , y , and z directions, respectively, to overcome the finite size effect (SI, III). As shown in Fig. 4, the thermal conductivity of BDTMC shows a very weak temperature dependence over the temperature range considered (100 - 350 K). This weak temperature dependence is normally observed at high temperature limit, well within the validity of classical MD simulation. We get a value of 0.34 ± 0.02 W/m-K at 300 K, which falls into the common range of $0.1 \sim 1$ W/m-K for organic molecular crystals.²⁹⁻³¹

The low thermal conductivity originates from the weak intermolecular bonding of VDW nature, in contrast to the strong intramolecular valence bonding. Different kinds of bonds result in very different frequency/time scales of inter- and intra-molecular dynamics. The thermal conductivity of the molecular crystal is dominated by the low-frequency inter-molecular vibrations. Their frequency mismatch with the intra-molecular vibrations prevents efficient heat transport between molecules, good for thermoelectric performance. That is, most of the energy is localized inside

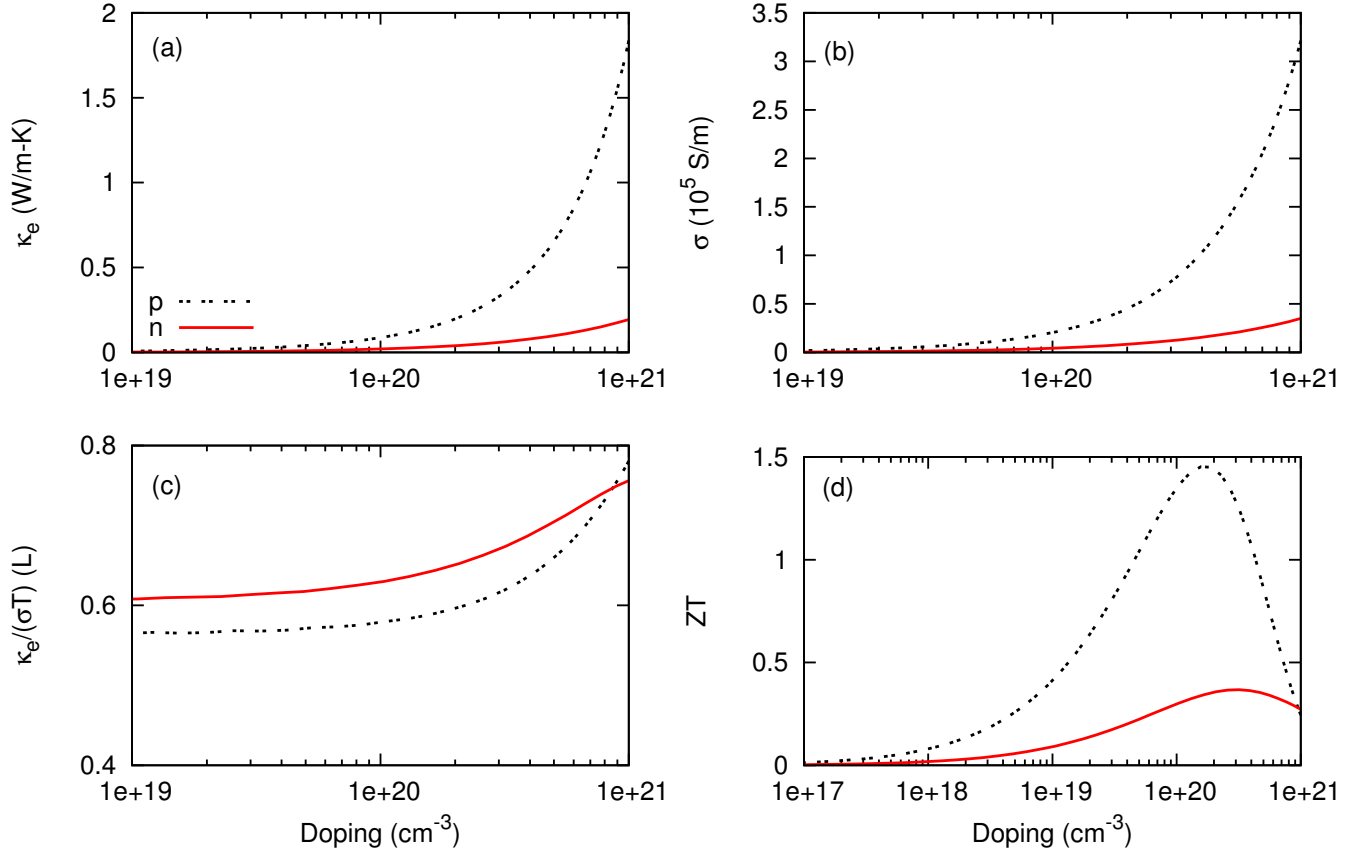


Figure 3: **Thermoelectric transport coefficients at 300 K.** (a)-(b) The electron thermal conductivity κ_e and electrical conductivity σ as a function of electron (n) and hole (p) doping. (c) $\kappa_e/(\sigma T)$ as a function of doping, in unit of the Lorentz number $L = \pi^2 k_B^2 / (3e^2)$, such that the Wiedemann-Franz law corresponds to $\kappa_e/(\sigma T) = L$. (d) ZT as a function of doping.

each molecule, instead of transferred to other molecules. This can be seen from the large overshoot of κ_{ph} as a function of correlation time in Fig. S4.

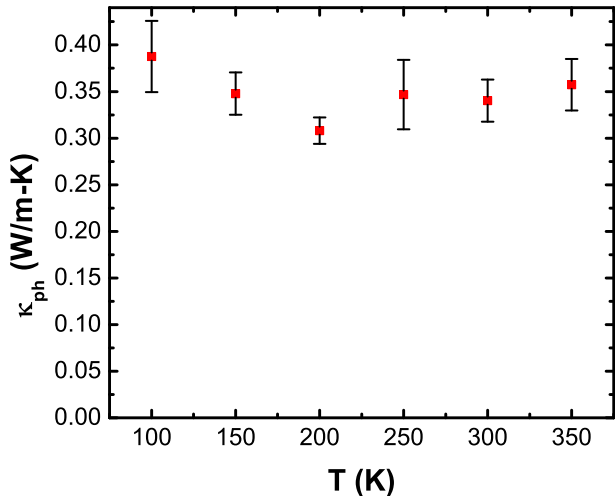


Figure 4: **Phonon thermal conductivity.** The phonon thermal conductivity as a function of temperature obtained from the classical molecular dynamics simulation.

Thermoelectric performance.

We are now in the position of evaluating the thermoelectric figure of merit ZT . As is shown in Fig 3(d), we get an optimal room-temperature ZT of 0.38 at electron doping of $\sim 3.2 \times 10^{20} \text{ cm}^{-3}$, and 1.48 at hole doping of $\sim 1.57 \times 10^{20} \text{ cm}^{-3}$. The corresponding Seebeck coefficients are $-199 \mu\text{V/K}$ for electrons and $266 \mu\text{V/K}$ for holes. The electron and hole mobility at optimal doping are ~ 2.4 and $\sim 12.8 \text{ cm}^2/\text{V-s}$, respectively. These results are summarized in Table 1. The following facts are note-worthy: (1) Although doping the organic semiconductors is still challenging in experiments, the optimal doping level we obtained here has been achieved in Pentacene experimentally;⁵³ (2) A much higher carrier mobility has been experimentally observed in C8-BTBT;⁵⁴ (3) Although the optimal electrical conductivity we obtained here has not been realized so far (the highest experimental value that can be achieved³¹ is $\sim 11000 \text{ S/m}$), there is no fundamental difficulty in realizing both (1) and (2) in the same material; (4) On the other hand, a recent study

shows that it is possible to reduce the optimal doping by increasing the carrier mobility.⁵⁵ Finally, in Fig. 5, we plot the temperature dependence of ZT . It shows an approximately linear dependence on T . We have checked that ZT saturates at higher T (Fig. S6). Since band-like transport at high T is questionable, we did not show it here. The ZT value is promising over a wide temperature range (100 - 350 K).

Table 1: Summary of important parameters and results for the conduction (CB) and valence band (VB): t the hopping element in the 1D model, m^* effective mass, D deformation potential, μ mobility at optimal doping, S Seebeck coefficient at optimal doping (n).

	t (eV)	m^* (m_0)	D (eV)	n (10^{20} cm^{-3})	ZT	μ ($\text{cm}^2/\text{V}\cdot\text{s}$)	S ($\mu\text{V}/\text{K}$)	κ_e ($\text{W}/\text{m}\cdot\text{K}$)
CB	0.05 (0.08)	4.27	-6.67	3.19	0.38	2.4	-199	0.06
VB	0.2	-1.5	-8.55	1.57	1.48	12.8	266	0.15

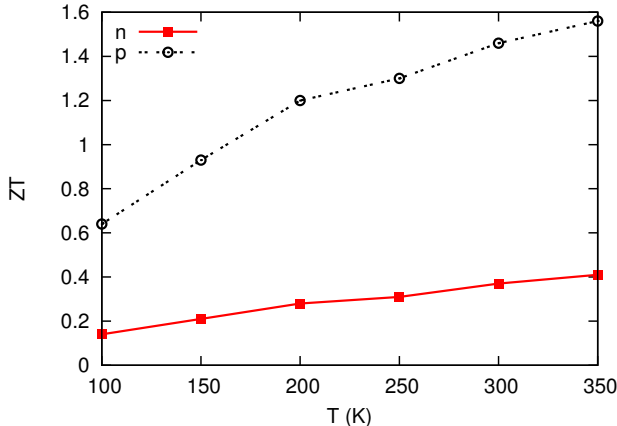


Figure 5: **Temperature dependence of ZT at optimal doping.**

The Q1D electrical transport and low phonon thermal conductivity we obtained here originate from the chemical nature of the inter-molecular bonding. In our calculation, the conduction and valence band structures of BDTMC are determined by only one parameter, t , reflecting the strength of the π - π VDW bonding. By comparing results of the CB and VB, we deduce that stronger bonding, thus larger t , results in better thermoelectric performance.

Our results, together with recent development in chemical control of the stacking angle and distance,^{26,38} point out possible way of further enhancing the thermoelectric performance by chemical or strain engineering of π - π overlap integral. DFT calculation confirms this idea. Within lattice

strain of 5%, we can achieve more than 20% change of t (Fig. S2).

Before closing, we should mention that, as doping is increased, the impurity scattering rate is also increased proportionally to the dopant concentration, resulting in a decrease σ and κ_e . But their ratio should not change much. Considering $ZT = S^2/(\kappa_e/\sigma T + \kappa_{ph}/\sigma T)$, we expect the ZT to be smaller after including the impurity scattering. But to include it quantitatively, we need to consider the screening of charged impurity, which depends on the dimension and dispersion of the electronic band structure. Since the main idea of this work does not rely on these details, we leave them to future study.

Conclusions

To summarize, we propose a novel approach to search for highly-efficient thermoelectric materials. That is to explore or engineer low-dimensional electronic structure in phonon-glass bulk crystals. Through atomistic simulation, we have shown that the π - π stacking molecular crystals are particularly suitable for such an approach. Both low phonon thermal conductivity and 1D electronic structure originate from the π - π bonding. Besides proving the principle, our results also show the promising potential of π - π stacking organic crystals as efficient thermoelectric material. Although we only considered organic crystals in this work, the idea should be equally applicable to inorganic materials. Indeed, during the preparation of this work we became aware of a recent work, exploring similar idea in inorganic compounds.⁵⁶

Acknowledgements

J.-T.L. acknowledges stimulate discussions with members of the Danish-Chinese center for molecular nanoelectronics, from which the idea was initialized. J.-T.L. was supported by the National Natural Science Foundation of China (Grant No. 11304107 and 61371015). N.Y. was supported by the National Natural Science Foundation of China (Grant No.11204216), and the Self-Innovation Foundation of HUST (Grant No.2014TS115). The authors thank the National Supercomputing

Center in Tianjin (NSCC-TJ) and Shanghai, the High Performance Computing Center experimental testbed in SCTS/CGCL for providing help in computations.

References

- (1) Snyder, G. J.; Toberer, E. S. *Nat. Mater.* **2008**, *7*, 105–114.
- (2) Chen, G.; Dresselhaus, M. S.; Dresselhaus, G.; Fleurial, J.-P.; Caillat, T. *Int. Mater. Rev.* **2003**, *48*, 45–66.
- (3) Dresselhaus, M. S.; Chen, G.; Tang, M. Y.; Yang, R. G.; Lee, H.; Wang, D. Z.; Ren, Z. F.; Fleurial, J. P.; Gogna, P. *Adv. Mater.* **2007**, *19*, 1043–1053.
- (4) Dubi, Y.; Di Ventra, M. *Rev. Mod. Phys.* **2011**, *83*, 131–155.
- (5) Hicks, L. D.; Dresselhaus, M. S. *Phys. Rev. B* **1993**, *47*, 12727–12731.
- (6) Hicks, L. D.; Dresselhaus, M. S. *Phys. Rev. B* **1993**, *47*, 16631–16634.
- (7) Mahan, G. D.; Sofo, J. O. *Proc. Natl. Acad. Sci. U.S.A.* **1996**, *93*, 7436–7439.
- (8) Li, N.; Ren, J.; Wang, L.; Zhang, G.; Hänggi, P.; Li, B. *Rev. Mod. Phys.* **2012**, *84*, 1045–1066.
- (9) Wang, J.-S.; Wang, J.; Lü, J. T. *Euro. Phys. J. B* **2008**, *62*, 381–404.
- (10) Hochbaum, A. I.; Chen, R.; Delgado, R. D.; Liang, W.; Garnett, E. C.; Najarian, M.; Majumdar, A.; Yang, P. *Nature* **2008**, *451*, 163–167.
- (11) Boukai, A. I.; Bunimovich, Y.; Tahir-Kheli, J.; Yu, J.; Goddard III, W. A.; Heath, J. R. *Nature* **2008**, *451*, 168–171.
- (12) Markussen, T.; Jauho, A.; Brandbyge, M. *Phys. Rev. Lett.* **2009**, *103*, 055502.
- (13) Brovman, Y. M.; Small, J. P.; Hu, Y.; Fang, Y.; Lieber, C. M.; Kim, P. *arXiv:1307.0249* **2013**,

- (14) KirÅaanskas, G.; Li, Q.; Flensberg, K.; Solomon, G. C.; Leijnse, M. *Appl. Phys. Lett.* **2014**, *105*, 233102.
- (15) Zhao, L.-D.; Dravid, V. P.; Kanatzidis, M. G. *Energ. Environ. Sci.* **2014**, *7*, 251–268.
- (16) Poudel, B.; Hao, Q.; Ma, Y.; Lan, Y.; Minnich, A.; Yu, B.; Yan, X.; Wang, D.; Muto, A.; Vashaee, D.; Chen, X.; Liu, J.; Dresselhaus, M. S.; Chen, G.; Ren, Z. *Science* **2008**, *320*, 634–638.
- (17) Biswas, K.; He, J.; Zhang, Q.; Wang, G.; Uher, V. P. K. M. G., Ctirad Dravid *Nat. Chem.* **2011**, *3*, 160–166.
- (18) Yu, B.; Zebarjadi, M.; Wang, H.; Lukas, K.; Wang, H.; Wang, D.; Opeil, C.; Dresselhaus, M.; Chen, G.; Ren, Z. *Nano Lett.* **2012**, *12*, 2077–2082, PMID: 22435933.
- (19) Zhao, L.-D.; Lo, S.-H.; Zhang, Y.; Sun, H.; Tan, G.; Uher, C.; Wolverton, C.; Dravid, V. P.; Kanatzidis, M. G. *Nature* **2014**, *508*, 373–377.
- (20) Koumoto, K.; Wang, Y.; Zhang, R.; Kosuga, A.; Funahashi, R. *Annu. Rev. Mater. Res.* **2010**, *40*, 363.
- (21) Jiang, J.-W.; Yang, N.; Wang, B.-S.; Rabczuk, T. *Nano Lett.* **2013**, *13*, 1670–1674, PMID: 23517486.
- (22) Yang, L.; Yang, N.; Li, B. *Nano Lett.* **2014**, *14*, 1734–1738.
- (23) Parida, B.; Iniyan, S.; Goic, R. *Renew. Sust. Energ. Rev.* **2011**, *15*, 1625 – 1636.
- (24) Kalyani, N. T.; Dhoble, S. *Renew. Sust. Energ. Rev.* **2012**, *16*, 2696 – 2723.
- (25) Dimitrakopoulos, C.; Malenfant, P. *Adv. Mater.* **2002**, *14*, 99–117.
- (26) Dong, H.; Fu, X.; Liu, J.; Wang, Z.; Hu, W. *Adv. Mater.* **2013**, *25*, 6158–6183.
- (27) Zhang, L.; Tan, L.; Hu, W.; Wang, Z. *J. Mater. Chem.* **2009**, *19*, 8216–8222.

- (28) Zhang, L.; Tan, L.; Wang, Z.; Hu, W.; Zhu, D. *Chem. Mater.* **2009**, *21*, 1993–1999.
- (29) Wang, D.; Shi, W.; Chen, J.; Xi, J.; Shuai, Z. *Phys. Chem. Chem. Phys.* **2012**, *14*, 16505–16520.
- (30) Chen, J.; Wang, D.; Shuai, Z. *J. Chem. Theory Comput.* **2012**, *8*, 3338–3347.
- (31) Zhang, Q.; Sun, Y.; Xu, W.; Zhu, D. *Adv. Mater.* **2014**, *26*, 6829–6851.
- (32) Casian, A. I.; Sanduleac, I. I. *J. Thermoelectricity* **2013**, *3*, 11–20.
- (33) Leclerc, M.; Najari, A. *Nat. Mater.* **2011**, *10*, 409–410.
- (34) Mateeva, N.; Niculescu, H.; Schlenoff, J.; Testardi, L. R. *J. Appl. Phys.* **1998**, *83*, 3111–3117.
- (35) Pfeiffer, M.; Beyer, A.; Fritz, T.; Leo, K. *Appl. Phys. Lett.* **1998**, *73*, 3202–3204.
- (36) Yue, R.; Xu, J. *Synthetic Metals* **2012**, *162*, 912–917.
- (37) Kim, G.-H.; Shao, L.; Zhang, K.; Pipe, K. P. *Nat. Mater.* **2013**, *12*, 719–723.
- (38) Giri, G.; Verploegen, E.; Mannsfeld, S. C. B.; Atahan-Evrenk, S.; Kim, D. H.; Lee, S. Y.; Becerril, H. A.; Aspuru-Guzik, A.; Toney, M. F.; Bao, Z. *Nature* **2011**, *480*, 504–508.
- (39) Ozturk, T.; Ertas, E.; Mert, O. *Tetrahedron* **2005**, *61*, 11055 – 11077.
- (40) Sirringhaus, H.; Friend, R. H.; Li, X. C.; Moratti, S. C.; Holmes, A. B.; Feeder, N. *Appl. Phys. Lett.* **1997**, *71*, 3871–3873.
- (41) Jiang, X.; Wei, Z.; Hu, W.; Qiu, X. private communications.
- (42) Kresse, G.; Furthmüller, J. *Comp. Mater. Sci.* **1996**, *6*, 15–50.
- (43) Perdew, J.; Burke, K.; Ernzerhof, M. *Phys. Rev. Lett.* **1996**, *77*, 3865–3868.
- (44) Grimme, S. *J. Comput. Chem.* **2004**, *25*, 1463–1473.

- (45) Coropceanu, V.; Cornil, J.; da Silva Filho, D. A.; Olivier, Y.; Silbey, R.; Brédas, J.-L. *Chem. Rev.* **2007**, *107*, 926–952.
- (46) Pernstich, K. P.; Rüßner, B.; Batlogg, B. *Nat. Mater.* **2008**, *7*, 321–325.
- (47) Kobayashi, H.; Kobayashi, N.; Hosoi, S.; Koshitani, N.; Murakami, D.; Shirasawa, R.; Kudo, Y.; Hobara, D.; Tokita, Y.; Itabashi, M. *J. Chem. Phys.* **2013**, *139*, 014707.
- (48) Tan, L.; Zhang, L.; Jiang, X.; Yang, X.; Wang, L.; Wang, Z.; Li, L.; Hu, W.; Shuai, Z.; Li, L.; Zhu, D. *Adv. Funct. Mater.* **2009**, *19*, 272–276.
- (49) Madsen, G. K. H.; Singh, D. J. *Comput. Phys. Commun.* **2006**, *175*, 67–71.
- (50) Bardeen, J.; Shockley, W. *Phys. Rev.* **1950**, *80*, 72–80.
- (51) Beleznyay, F. B.; Bogdan, F.; Ladik, J. *J. Chem. Phys.* **2003**, *119*, 5690–5695.
- (52) Plimpton, S. *Journal of Computational Physics* **1995**, *117*, 1–19.
- (53) Hayashi, K.; Shinano, T.; Miyazaki, Y.; Kajitani, T. *J. Appl. Phys.* **2011**, *109*, 023712.
- (54) Yuan, Y.; Giri, G.; Ayzner, A. L.; Zoombelt, A. P.; Mannsfeld, S. C. B.; Chen, J.; Nordlund, D.; Toney, M. F.; Huang, J.; Bao, Z. *Nat. Commun.* **2014**, *5*, 3005.
- (55) Shi, W.; Chen, J.; Xi, J.; Wang, D.; Shuai, Z. *Chem. Mater.* **2014**, *26*, 2669–2677.
- (56) Bilc, D. I.; Hautier, G.; Waroquiers, D.; Rignanese, G.-M.; Ghosez, P. *Phys. Rev. Lett.* **2015**, *114*, 136601.